A high-speed retro-reflector for free-space communication based on electro-optic phase modulation

T. Mikaelian, M. Weel, A. Kumarakrishnan, P.R. Battle, and R.C. Swanson

Abstract: We demonstrate that an electro-optic phase modulator (EOM) can be used as a constituent of a corner-cube-based modulated high-speed retro-reflector. We performed experiments to investigate the efficiency of the phase modulation produced by an EOM as a function of the angle of a laser beam incident on it. Our experiments demonstrate that the field of view of the EOM is determined by its dimensions and the diameter of the laser beam. This suggests that the device may be suitable for applications involving high-speed (GHz), free-space communication. In these applications, the retro-reflector can be mounted on a moving platform such as a satellite. We find that it is possible to detect the retro-reflected signal with an adequate signal-to-noise ratio using heterodyne detection. We also discuss some practical considerations necessary for the implementation of such a device.

PACS Nos.: 42.60.–V, 42.62.Cf, 42.62.Fi, 42.79.Sz, 42.79.Hp

Résumé : Nous avons démontré qu'un modulateur de phase magnéto-optique (EOM) peut être utilisé comme constituent d'un rétro-réflecteur modulé à haute vitesse basé sur un réflecteur en coin. Nous avons fait des mesures pour étudier l'efficacité de la modulation de phase produite par un EOM, en fonction de l'angle du rayon laser incident. Nos expériences montrent que le champ de vision de l'EOM est déterminé par ses dimensions et par le diamètre du faisceau laser. Ceci suggère que le dispositif peut être utilisé dans des applications impliquant des communications à haute vitesse (GHz) dans l'espace libre. Dans ces applications, le rétro-réflecteur peut être monté sur une plate-forme mobile comme un satellite. Nous observons que l'utilisation d'un récepteur hétérodyne permet de détecter le signal rétro-réfléchi avec un niveau adéquat du rapport signal sur bruit. Nous discutons aussi certaines considérations pratiques nécessaires à la réalisation d'un tel dispositif.

[Traduit par la Rédaction]

Received 31 May 2002. Accepted 20 November 2002. Published on the NRC Research Press Web site at http://cjp.nrc.ca/ on 5 June 2003.

T. Mikaelian, M. Weel, and A. Kumarakrishnan.[1] Department of Physics and Astronomy, York University, 4700 Keele St., Toronto, ON M3J 1P3, Canada.
P.R. Battle. AdvR Inc., Advanced Technology Park, 910 Technology Blvd., Suite K, Bozeman, MT 59718, U.S.A.
R.C. Swanson. Resonon Inc., 611 N. Wallace #7, Bozeman, MT 59715, U.S.A.

[1]Corresponding author (e-mail: akumar@yorku.ca).

 doi: 10.1139/P03-051

Fig. 1. Remote module consisting of collection optics, EOM, and retro-reflector.

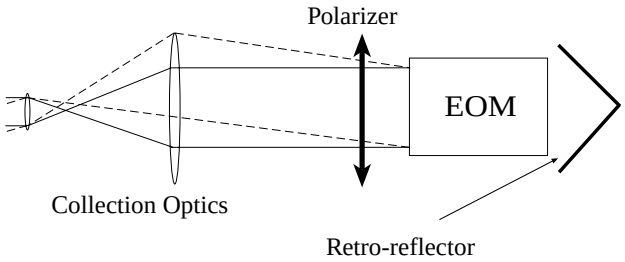

1. Introduction

During the last few years, it has been possible to demonstrate optical-fiber-based communication at bit rates of 40 Gb/s. However, there is an increasing interest in achieving high-speed optical communication in free space, since it may offer cost-efficient solutions in certain cases [1]. Examples where this may be effective include communication between high-rise towers, temporary communication terminals, relay stations on hazardous industrial floors, and communication with moving platforms such as satellites.

A modulated corner-cube retro-reflector for free-space communication has recently been proposed and tested [2]. This device is based on the modulation of the intensity of a laser passing through liquid-crystal sheets. Although it has some desirable characteristics such as small size, low power consumption, and large acceptance angle ($\sim$15°), it operates at a rate of $\sim$10 kHz and is not capable of high-speed data communication. Reference 3 describes a compact modulated retro-reflector that can communicate at a much higher rate ($\sim$10 MHz). This device is based on a multiple quantum well modulator. Although it has a field of view of $\sim$20°, the on–off contrast ratio depends on the fabrication process and varies between 2:1 and 4:1.

Other methods of achieving high-speed ($\sim$GHz) modulated retro-reflectors involve the use of acousto-optic modulators (AOM) [4] and electro-optic phase modulators (EOM) [5, 6] (as in this work). In particular, the EOM-based retro-reflector relies on detecting the retro-reflected signal by the presence or absence of frequency sidebands. As a result, heterodyne techniques are used for signal detection. In this case, the signal can be measured with a high signal-to-noise ratio against a zero background. The advantages of using FM techniques for free-space communication have been addressed in ref. 7.

For most applications, the driver of the EOM must be compact and provide sufficient power for phase modulation. The device discussed in this paper meets these requirements.

The EOM-based device primarily consists of a source module with a CW (continuous wave) laser and a detection system, and a remote module consisting of collection optics, an EOM, and a corner-cube reflector (see Fig. 1). To communicate a data stream to the source module, radio frequency (RF) pulses are applied to the EOM. This results in a phase-modulated signal for the duration of the pulse. The phase-modulated beam is retro-reflected to the source module by a corner-cube reflector. The presence or absence of phase modulation can then be decoded and converted to a binary stream.

We performed a proof-of-concept experiment using an EOM operating at 2.9 GHz. This experiment demonstrated that variations in the angular position of the EOM do not affect the efficiency of phase modulation within the range of angles measured.

In contrast to the EOM-based device, the acceptance angle of the AOM-based retro-reflector [4] is not determined by the aperture of the AOM. As a consequence, the AOM-based device may require servo-control of optics and RF electronics for its implementation. The EOM-based device should be easier to implement, since the dimensions of the EOM and the laser beam define its acceptance angle. Additionally, the device is capable of achieving a communication rate of the order of the modulation rate of the EOM (several GHz).

Fig. 2. Phase-modulated/not-phase-modulated encoding of data bits with period T. Here, the phase-modulation rate is twice the rate of data encoding.

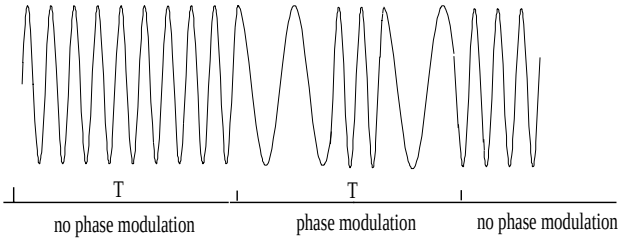

The rest of the paper is organized as follows. In Sect. 2, we discuss the principle of operation of this device. In Sect. 3 we present the results of proof-of-concept experiments. Finally, in Sect. 4, we evaluate issues related to the implementation of the device.

2. Principle of operation

2.1. Electro-optic phase modulation

Phase modulation produced by an EOM is the result of variations in the index of refraction of the crystal. This variation is due to changes in the electric field produced by a RF modulation. The modulation results in frequency sidebands in the spectrum of the laser, but it does not significantly modulate the laser intensity. To optimize the effect of phase modulation, the polarization of the laser beam must be aligned with the birefringent axis of the EOM. A polarizing sheet placed in front of the EOM will serve this purpose. Once the incoming beam is polarized along the correct axis, the phase modulator can be expected to be largely insensitive to variations in the angle of incidence.

When a RF voltage is applied to the EOM, the laser beam will be phase modulated. The EOM driver must modulate the voltage at a rate higher than the data-encoding rate. Thus, the communication rate of an EOM-based retro-reflector is limited by the operating frequency of the EOM. Figure 2 illustrates such an encoding with a phase-modulation rate that is twice the rate of data encoding.

The electric field of the laser beam after passing through the EOM is expressed in complex notation as [8]

$$E(t) = E_{\mathrm{o}} \sum_{m=-\infty}^{m=\infty} J_m(M) \exp\left[i\left(w_{\mathrm{L}} + m w_{\mathrm{RF}}\right) t\right] \tag{1}$$

Here, E_{o} is the incident amplitude, J_m is the Bessel function of order m, w_{L} is the optical carrier frequency, and w_{RF} is the radio frequency of the EOM driver. The modulation index M is defined as the peak phase shift $\Delta\phi$ induced when a voltage is applied to an electro-optic phase modulator and is given by

$$M = \Delta\phi = \frac{\pi}{\lambda} n^3 r_{33} \sqrt{\frac{2PQl}{w_{\mathrm{RF}} \epsilon h d}} \tag{2}$$

where λ is the wavelength of the laser, n is the unperturbed index of refraction of the EOM crystal, r_{33} is the Pockels coefficient, l is the length of the EOM crystal, d and h are the width and height of the crystal, respectively, ϵ is the dielectric constant of the crystal, Q is the quality factor of the EOM cavity, P is the RF power applied to the EOM, and w_{RF} is the EOM frequency. Equations (1) and (2) can be used to describe the amplitude of the frequency sidebands that are produced when the EOM is pulsed.

Fig. 3. Source module consisting of laser and detection system. A small portion of the primary laser beam is diverted and frequency shifted (using an AOM) for use as a local oscillator.

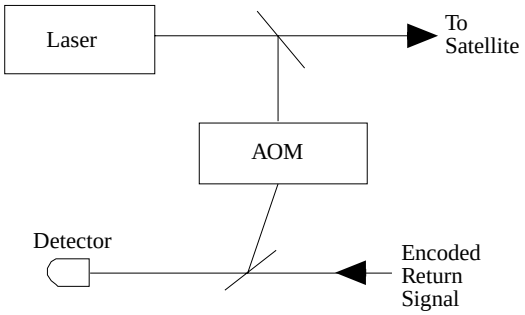

Fig. 4. Spectral components incident on the detector with (*a*) no phase modulation and (*b*) phase modulation.

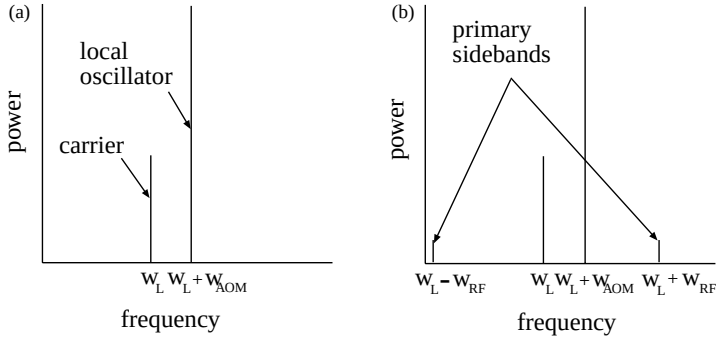

2.2. Signal detection

The retro-reflected signal has frequency sidebands when the EOM is on, and no sidebands when the EOM is off. As a result, it is possible to achieve a 100% on–off contrast ratio, i.e., a zero background, by using a well-established technique such as heterodyne detection. The zero background results from the fact that the sidebands are spectrally distinct from the laser carrier frequency w_{L}.

Because optical frequencies are several orders of magnitude too large to be detected, the phase modulation shown in Fig. 2 cannot be directly observed. Signal detection can be accomplished by mixing the return beam with a strong local oscillator thereby allowing the detection of the resulting beat signal with near shot-noise limited performance.

This concept is illustrated schematically in Fig. 3. A small portion of the primary laser beam is diverted into an AOM. The AOM upshifts the frequency w_{L} of the beam by the frequency w_{AOM} of the AOM driver. This beam, referred to as the "local oscillator", is mixed with the retro-reflected signal on a high-speed photodiode. If the signal beam has not been phase modulated, the spectrum of the light incident on the detector will have two distinct frequency components: one from the signal (w_{L}), and the other from the local oscillator ($w_{\mathrm{L}} + w_{\mathrm{AOM}}$), as shown in Fig. 4*a*. The only frequency that will be detected is the difference between the local oscillator frequency $w_{\mathrm{L}} + w_{\mathrm{AOM}}$ and the carrier frequency w_{L}. The intensity measured on the detector will be proportional to the terms given by

$$A_{\mathrm{L}}^2 \sin^2(w_{\mathrm{L}} t) + A_{\mathrm{LO}}^2 \sin^2(w_{\mathrm{L}} + w_{\mathrm{AOM}})t + A_{\mathrm{L}} A_{\mathrm{LO}}[\cos(w_{\mathrm{AOM}} t) - \cos(2w_{\mathrm{L}} + w_{\mathrm{AOM}})t] \tag{3}$$

Here, A_{L} and A_{LO} are the amplitudes of the carrier and local oscillator signals, respectively. Frequencies of the order of magnitude of w_{L} are not detected. Hence, the signal detected by the photodiode will be a pure sine wave (at a frequency w_{AOM}).

On the other hand, a phase-modulated beam will result in the spectrum shown in Fig. 4*b*. The primary

Fig. 5. Experimental setup for studying the field of view of the EOM.

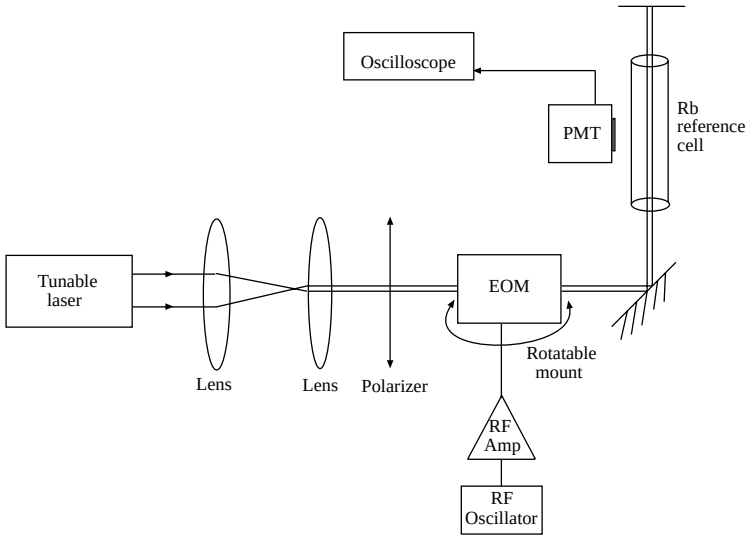

sideband frequencies in the retro-reflected beam are $w_{\mathrm{L}} - w_{\mathrm{RF}}$ and $w_{\mathrm{L}} + w_{\mathrm{RF}}$, where w_{RF} is the frequency of the EOM driver, (1). The local oscillator will beat with three spectral components ($w_{\mathrm{L}} - w_{\mathrm{RF}}$, w_{L}, and $w_{\mathrm{L}} + w_{\mathrm{RF}}$) as shown in Fig. 4*b*. In this case, the beat signal is a complicated wave form with three distinct detectable difference frequency components: w_{AOM}, $w_{\mathrm{RF}} - w_{\mathrm{AOM}}$, and $w_{\mathrm{RF}} + w_{\mathrm{AOM}}$. We note that the frequency term $w_{\mathrm{RF}} + w_{\mathrm{AOM}}$ is significantly higher than w_{AOM}. Consequently, the phase-modulated signal will have a higher frequency component than the non-phase-modulated signal. Thus, the presence of the phase modulation can be detected by using a high-pass filter, tuned to the desired frequencies (w_{AOM}, $w_{\mathrm{RF}} - w_{\mathrm{AOM}}$, and $w_{\mathrm{RF}} + w_{\mathrm{AOM}}$).

3. Proof of concept experiments

Ideally, retro-reflectors should have a large field of view. For example, in refs. 2 and 3, the field of view is typically ~15°. Since an important feature of the EOM-based device is its relative insensitivity to variations in the angle of incidence of the laser beam, we carried out a proof-of-concept experiment to investigate the field of view.

To determine the field of view, we measure the range of incident angles for which effective phase modulation could be observed. The experimental setup is shown in Fig. 5. We use a tunable 780 nm laser and a 2.915 GHz EOM with a 1 mm aperture for this experiment. The diameter of the laser beam is adjusted to be about 0.6 mm at the location of the EOM. The confocal beam parameter (3.6×10^2 mm) is larger than the length of the EOM crystal (10 mm). The EOM is fixed on a rotatable mount and the amplitude of the frequency sidebands produced by the phase modulation is monitored as a function of the EOM angle.

It is possible to measure the intensity of the sidebands using a spectrum analyzer or a Fabry–Perot cavity. However, our technique is unusual, and involves scanning the laser frequency and observing fluorescence at a right angle from a Rb reference cell at room temperature. We, therefore, describe the technique in detail. The advantage of this technique is that it is relatively inexpensive and the measurement can be carried out without using high-speed electronics.

The Rb reference cell contains a naturally occurring mixture of ^{85}Rb and ^{87}Rb isotopes in the ratio 72:28. The atomic level structures for ^{85}Rb and ^{87}Rb are shown in Fig. 6. The EOM-driver frequency w_{RF} is tuned to ~2.915 GHz, which is the frequency difference between the $F = 2$ to $F' = 3$ and $F = 3$ to $F' = 4$ transitions. As the laser frequency is scanned with the EOM turned off, the laser frequency is

Fig. 6. Atomic energy level structure of ^{85}Rb and ^{87}Rb.

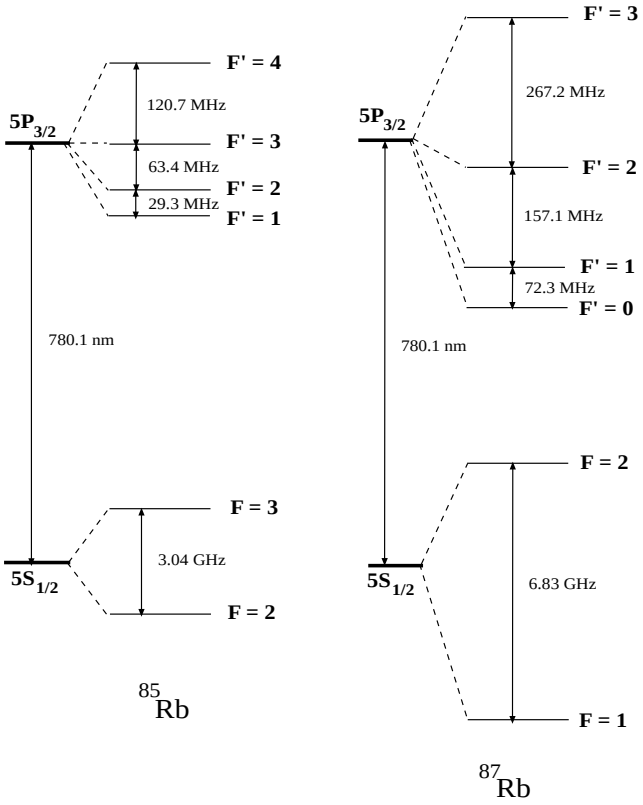

successively in resonance with four Doppler-broadened transitions from the ground states of the two Rb isotopes. As a result, four fluorescence peaks corresponding to these transitions are observed (broken line in Fig. 7). When the EOM is turned on, new frequencies (corresponding to the sideband frequencies) are introduced in the laser beam. When the laser is scanned, we observe changes in the amplitude of the fluorescence peaks, as well as additional peaks in the fluorescence spectrum (continuous line in Fig. 7). The intensity of the fluorescence of the Doppler broadened $F = 2$ to $F' = 1$, 2, and 3 transition in ^{85}Rb is observed to increase. This is because when the carrier frequency is on resonance with the $F = 2$ to $F' = 1$, 2, and 3 transition, its lower sideband is on resonance with a strong transition ($F = 3$ to $F' = 2$, 3, and 4 transition in ^{85}Rb). On the other hand, the fluorescence of the $F = 3$ to $F' = 2$, 3, and 4 transition in ^{85}Rb is observed to decrease. This is because when the carrier frequency is on resonance with the $F = 3$ to $F' = 2$, 3, and 4 transition, a fraction of the carrier intensity is transferred to the sidebands and the upper sideband is in resonance with a weaker transition ($F = 2$ to $F' = 1$, 2, and 3 in ^{85}Rb).

When the laser frequency is at point A, marked in Fig. 7 (EOM off), we note that it is not on resonance with any of the Doppler-broadened transitions. When the EOM is on and the laser frequency is at point A, its lower sideband frequency is on resonance with the $F = 2$ to $F' = 1$, 2, and 3 transition in ^{87}Rb. Therefore, the additional peak observed at point A in Fig. 7 is due to the sideband alone. It can, therefore, be used for measuring the efficiency of phase modulation.

We use experimental parameters of $l = 780$ nm, $n = 2.18$, $r_{33} = 31 \times 10^{-12}$, and $\epsilon = 3.8 \times 10^{-10}$ C^2/J m for a MgO-doped $LiNbO_3$ EOM crystal, $l = 10$ mm and $d = h = 1$ mm to estimate the modulation index using (3). Here, we note that d and h are the effective width and height of the

Fig. 7. Oscilloscope traces of the fluorescence signal observed as the laser frequency is scanned. The broken line is observed when the EOM is off. The continuous line is observed when the EOM is on. $\Delta = 2.915$ GHz.

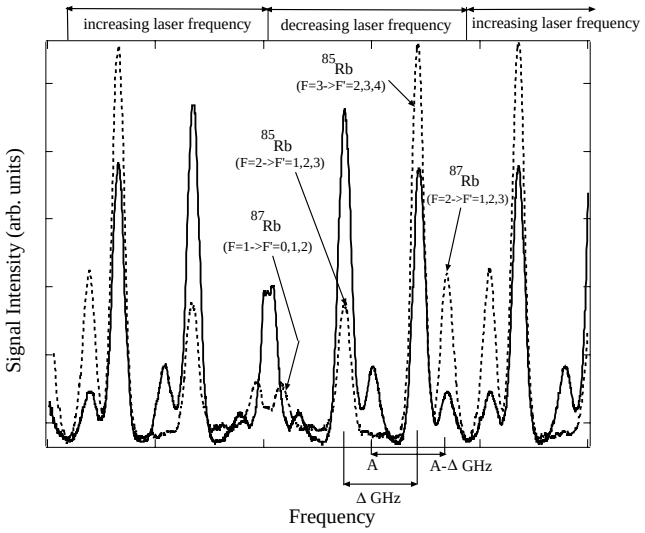

Fig. 8. Fluorescent intensity as a function of laser intensity. From the fit, a saturation intensity of 18.8 mW/cm^2 is obtained.

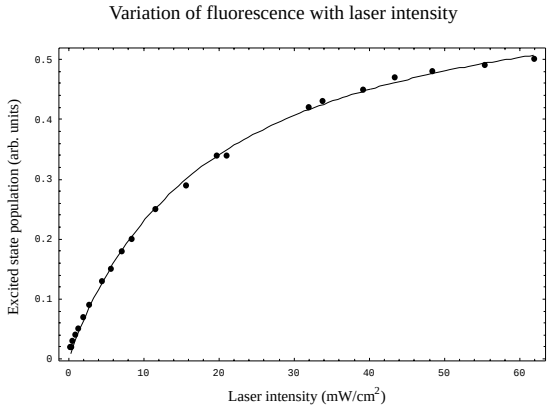

crystal, as determined by the EOM aperture. We used a RF power of 1 W in the experiments. Using a Q factor of 422 for the EOM cavity (as specified by the manufacturer), we estimate a peak voltage of $\sim$108 V across the EOM crystal. This gives a modulation index $M = 1.47$. From (1), the fraction of power transferred to each of the first-order sidebands is $[J_1(1.47)]^2 = 0.306$. The fraction of power that remains in the carrier is $[J_o(1.47)]^2 = 0.279$. These estimates are consistent with the amplitude of the sidebands measured in the experiment (Fig. 7).

The measurement of the efficiency of phase modulation due to angular variations of the EOM relies on measuring changes in the fluorescence, and relating it to the intensity of the sidebands. Since the fluorescence is proportional to the number of atoms N_1 in the excited state, it is necessary to ensure that we perform the experiment under the condition that N_1 is linearly related to the laser intensity. Therefore, it is necessary not to saturate the atomic transition during the experiment.

To ensure this, we first studied the variation of fluorescence of the $F = 3$ to $F' = 2$, 3, and 4 Doppler-broadened transition peak as a function of laser intensity. The experimental data are shown in Fig. 8. For a two-level atom, the number of atoms in the excited state can be obtained by using the

Fig. 9. Schematic diagram showing angular variations of the EOM in (*a*) the horizontal plane and (*b*) the vertical plane.

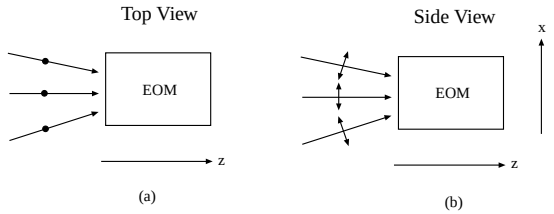

optical Bloch equations [9] assuming that the system is in a steady state. The fraction f of atoms in the excited state is given by

$$f = \frac{N_1}{N_0 + N_1} = \frac{\left(\frac{I}{I_s}\right)}{2\left(\frac{I}{I_s}\right) + 4\left(\frac{\Delta}{\Gamma}\right)^2 + 1} \tag{4}$$

where N_0 is the ground-state population, I is the laser intensity, I_s is the atomic saturation intensity, Δ is the laser detuning, and Γ is the natural linewidth of the atomic transition. Since we measure the amplitude at the fluorescence peak ($\Delta = 0$), we can express the number of atoms in the excited state as

$$N_1 = \frac{\left(\frac{I}{I_s}\right) N_0}{\frac{I}{I_s} + 1} \tag{5}$$

We fit the data in Fig. 8 to (5) to get $I_s = 18.8$ mW/cm^2. The estimated statistical uncertainty is less than 10%. The value from the fit is comparable to the calculated value of $I_s = 14.6$ mW/cm^2, obtained by using a weighted average of the saturation intensities of the $F = 3$ to $F' = 2$, 3, and 4 transitions. The calculation of the saturation intensities assumes that the magnetic sublevels of the ground state are equally populated. This assumption is valid for a sample at room temperature in zero magnetic field. The discrepancy can be attributed primarily to the uncertainty in the power measurements ($\pm$20%).

Based on these results, we operate the laser below the saturation intensity (typically 5–7 mW/cm^2) for measurements of the intensity of the sidebands as a function of the EOM angle. We measure the angular dependence of phase modulation in both the horizontal and vertical planes.

For angular variations of the EOM in the horizontal plane, the polarization is always in the same direction (see Fig. 9*a*), perpendicular to the direction of propagation (z axis) and parallel to the axis of the EOM. From geometrical considerations, we would expect the efficiency of phase modulation to be constant as a function of angle. However, when the angle changes, the path length through the crystal will be increased by a factor of $1/\cos\theta$, where θ is the angle between the z axis and the direction of propagation. According to (2), this effect will actually increase the amplitude of phase modulation slightly.

If there are angular changes in the vertical plane, the laser polarization has a component parallel to the propagation direction of the laser beam and a component parallel to the direction of the EOM axis (x axis in Fig. 9*b*). No phase modulation will occur for the component parallel to the propagation direction. Therefore, if the angular variations are large, the intensity of the sidebands will be reduced. However, this effect is relatively small ($\sim$25% reduction) even for angular variations of $\sim$15°.

The experimental data for the angular changes in the horizontal plane are shown in Fig. 10*a*. We find the field of view to be $\sim$2°. The graph also shows the transmitted laser power as a function of angle. The transmitted power decreases to $1/e^2$ of its peak value over a range of 2°. We, therefore, conclude that the sideband intensity begins to decrease at the angular positions at which the laser beam starts clipping the edge of the EOM aperture. The experimental data for angular variations in the vertical plane are

Fig. 10. Angular variations of the EOM in the (*a*) horizontal plane and (*b*) vertical plane. The continuous lines represent the sideband intensity as a function of the EOM angle. The broken lines represent variations in the power of the laser.

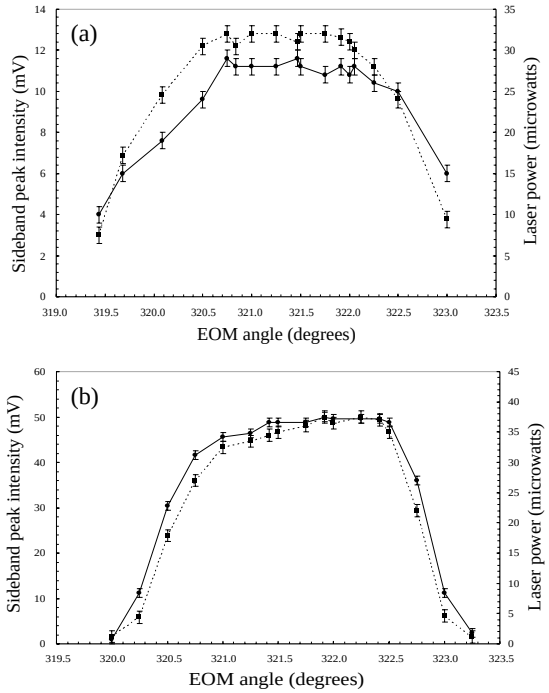

shown in Fig. 10*b*. Once again, the range of angles for which the laser beam is not clipped by the EOM aperture is ∼2°. Over this range, the sideband intensity is essentially unchanged.

From geometry, if the laser beam is incident on the EOM at a small angle, the field of view of the EOM in a given plane can be estimated to be

$$\theta = 2\tan^{-1}\left(\frac{A+D}{L}\right) \tag{6}$$

where A is the dimension of the square EOM aperture ($A = 1$ mm), D is the $1/e^2$ diameter of the Gaussian laser beam ($D = 0.6$ mm), and L is the length of the EOM module ($L = 30$ mm). We calculate θ to be 1.53°. This estimate has to be corrected to account for the lateral displacement of the beam due to refraction through the EOM crystal (crystal length $l = 10$ mm). The corrected estimate is ∼2°, which is in agreement with the measured value for the field of view. The experiment indicates that the field of view is primarily defined by the dimensions of the EOM aperture, the length of the EOM module, and the diameter of the laser beam. These results suggest that an EOM can potentially be used in a high-speed retro-reflector mounted on a moving platform. Further experiments with larger aperture EOMs should be performed to investigate the possibility of obtaining a field of view of ∼15°, as in refs. 2–4.

4. Practical considerations

We now discuss some issues related to the implementation of the device, including RF-power requirements, the design of collection optics for increasing the field of view, the optical power requirements for the detection system, and a simple scheme for decoding the data.

Fig. 11. RF power calculated as a function of the percentage of carrier power transferred to the first-order sideband. The squares correspond to a field of view of 20°; the circles correspond to a field of view of 1.5°.

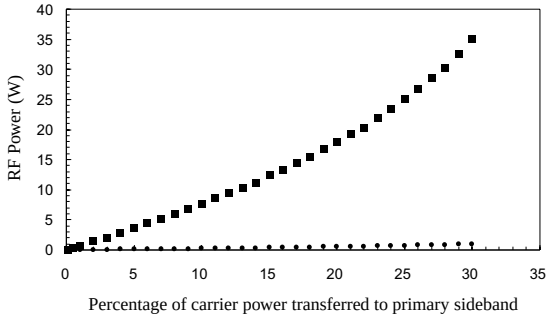

4.1. RF-power requirements

We now calculate the power requirements for a high-speed EOM with a large field of view. Since the method of detection outlined in this paper is capable of detecting a sideband intensity of ∼0.1% of the incident intensity (with a signal-to-noise ratio of ∼1) [4], we first calculate the lower limit for the modulation index to be ∼0.07 (assuming we want to detect the primary sideband). For the EOM used in the experiment, a field of view of ∼20° can be obtained if the EOM aperture is increased to ∼5.9 mm, using a laser beam of 0.6 mm diameter. Using (2) and (6), we calculate the RF power required to be ∼0.08 W, which is very modest. Figure 11 illustrates the variation in the RF drive power as a function of the percentage of carrier power transferred to the first-order sidebands. The squares correspond to a field of view of 20°, and the circles correspond to a field of view of 1.5°. It is clear that for high sideband intensities, increasing the field of view requires a substantial increase in the RF power. Assuming that the signal-to-noise ratio is ∼1 if the sideband intensity is 0.1% of the carrier intensity, we estimate that a field of view of ∼20° can be achieved with a signal-to-noise ratio of ∼10, using a drive power of ∼1 W.

4.2. Local oscillator requirements

The source module will typically consist of an AOM to generate the local oscillator signal, and a high-speed photodiode (Fig. 3) as discussed in Sect. 2.

The amplitudes of the frequency components detected by the photodiode are proportional to the amplitude of both the local oscillator and the components it mixes with. Therefore, increasing the intensity of the local oscillator beam effectively amplifies the terms being detected. For a typical photodiode, the local oscillator power required for detection close to the shot-noise limit can be estimated to be approximately few milliwatts [10, 11]. This power level can be conveniently achieved using inexpensive diode lasers.

4.3. Decoding the data

There are several standard techniques for decoding a phase-modulated signal. Here, we outline a simple scheme for decoding the data as illustrated in Fig. 12. The figure shows the electronic components, as well as the evolution of the electrical signal as it passes through the stages of the decoder. The data stream (*a*) shown consists of three bits. The bits with high-frequency components have been phase modulated. In reality, the high-frequency regions of the signal will look more complicated than that depicted in Fig. 12 because of the presence of additional frequency components. The initial component of the decoder is a high-pass filter. If the cut-off frequency of the filter is set to be higher than w_{AOM} and lower than w_{RF}, wave form (*a*) will be transformed to wave form (*b*). To eliminate the high-frequency

Fig. 12. Schematic diagram of a simple decoding setup and the evolution of a modulated signal as it passes through various stages.

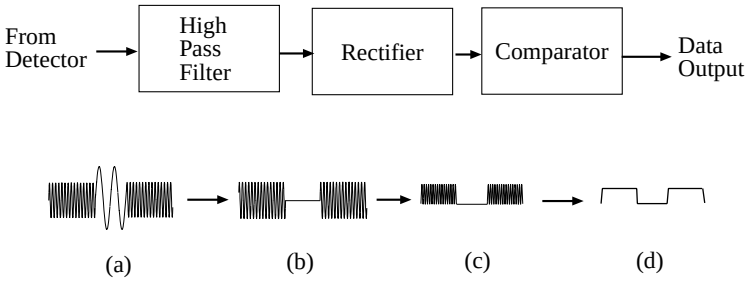

oscillation, the output from the high-pass filter is rectified (wave form (*c*)) and then turned into a standard bit stream using a comparator (wave form (*d*)).

5. Conclusions

We have performed an experiment to demonstrate the feasibility of using an EOM in a high-speed retro-reflector system for free-space communication. The experiment indicates that the intensity of phase modulation is relatively insensitive to angular variations. The field of view is defined primarily by the dimensions of the EOM and the spatial profile of the laser beam. Our results also show that the modulation rate can be several GHz, and that the signal can be detected against a zero background using heterodyne techniques. This is the main advantage of using this approach for a communication link.

Our calculations show that it is possible to obtain a field of view of $\sim 20^\circ$ using a modest RF power of <1 W. To increase the field of view and keep the RF power modest, it is necessary to build high-Q EOM cavities with large apertures (the system discussed in ref. 3 has an aperture of ~ 1 cm). A large aperture is necessary to ensure that the device performance is not limited by the return power. However, a high value of Q limits the usable bandwidth of the device. It is also interesting to note that as the angle of incidence α increases, the effective path length through the crystal increases as $1/\cos\alpha$. Correspondingly, the RF power required to produce the same modulation index (as for $\alpha = 0$) is smaller.

In conclusion, further studies remain to be carried out to establish that a field of view of $\sim 15^\circ$ is possible. Other challenges involve designing suitable collection optics that can enhance the field of view. The effects of beam distortion on the retro-reflected beam also need to be investigated. Furthermore, it may be necessary to design a suitable control system to maintain the polarization at the input to the EOM. However, the EOM-based device does not require any servo-control for the optics. We also note that the system can be designed so that only an authorized laser beam can be used to extract information from the device. For example, a coded pulse sequence can be used to initiate the data transmission. It is also necessary to estimate the laser power requirements for establishing a long-range communication link. Effects of laser beam propagation through the atmosphere can result in beam distortion and attenuation. To set up a communication link with a moving platform such as a satellite, it is necessary to implement a suitable tracking system. Although we do not address these issues, we note that they are common to all free-space communication devices [2, 3].

Acknowledgements

We acknowledge the contribution of A. Vorozcovs who wrote the software for the automated data acquisition. This research was supported by the Canada Foundation for Innovation, Ontario Innovation Trust, York University, and the Natural Sciences and Engineering Research Council of Canada.

References

1. J. Hecht. Laser Focus World, **11**, 101 (2001).
2. C.M. Swenson, C.A. Steed, I.A. De La Rue, and R.Q. Fugate. Proc. SPIE, **2990**, 296 (1997).
3. G.C. Gilbreath, W.S. Rabinovich, T.J. Meehan et al. Opt. Eng. **40**, 1348 (2001).
4. G. Spirou, I. Yavin, M. Weel, T. Mikaelian, A. Vorozcovs, A. Kumarakrishnan, P.R. Battle, and R.C. Swanson. Can J. Phys. **81**, 625 (2003).
5. T. Mikaelian, M. Weel, A. Kumarakrishnan, P.R. Battle, and R.C. Swanson. Presented at CUPC, Winnipeg, November 2001.
6. T. Mikaelian, M. Weel, A. Kumarakrishnan, P.R. Battle, and R.C. Swanson. Proceedings of the IEEE Aerospace Conference, Big Sky, Mont. 9–16 March 2002. IEEE Piscataway, N.J. Vol. 3, 1481 (2002).
7. R.R. Hayes. Appl. Opt. **40**, 6445 (2001).
8. M. Gehrtz, G. Bjorklund, and E. Whittaker. J. Opt. Soc. Am. B, **2**, 9 (1985).
9. H.J. Metcalf and P. van der Straten. Laser cooling and trapping. Springer, New York. 1999.
10. W.R. Leeb. Proc. SPIE, **1131**, 216 (1989).
11. R.A. Linke and A.H. Gnauck. J. Lightwave Technol. **LT-6**(11), 1750 (1988).